A Quantitative Cohesive Force Mechanism for Powder Flow: The Role of Metal Oxide Surface Additives in Xerographic Toner

Richard P. N. Veregin▲,* and Robert Bartha

Xerox Research Centre of Canada, Mississauga, Ontario, Canada

---

Xerographic toners use sub-micron metal oxide surface additives to control powder flow. Toner powder cohesion, which is inversely related to toner flow, was measured with respect to the primary particle size and surface chemistry of the oxide used as the flow additive. The cohesion data is interpreted in terms of a quantitative cohesive force mechanistic model for toner flow. Thus, cohesion is described in terms of Van der Waals, capillary, and hydrogen bonding forces between the oxide particles on the toner surfaces, and by the nanogeometry of the contact between oxide particles, controlled by the oxide primary particle size. Adhesion forces decrease, and thus flow improves, with decreasing oxide primary particle size and with increasing hydrophobicity.

Journal of Imaging Science and Technology 45: 571–578 (2001)

Introduction

This article studies adhesion of toner with surface oxides which are commonly used to control toner flow, charge,[1–5] and transfer.[6] While surface metal oxides are now nearly ubiquitous in toner applications, and have been used for many decades in the food and pharmaceutical industries, there is no work published to understand the mechanism of action of fine nanoparticles in controlling flow properties. In this article the toner cohesion with surface oxide additives was measured as a function of both the surface chemistry and the particle size of the oxide. A mechanistic model is developed, which describes the toner cohesion quantitatively in terms of fundamental adhesion forces, Van der Waals, capillary and hydrogen bonding forces, and the nanogeometry of the adhesive contact between metal oxide particles on the toner surfaces. The model describes well quantitatively the observed effects of the chemistry and the size of the oxide on the toner powder cohesion.

Experimental

Toner flow was measured on a Hosokawa Micron Powder tester using the standard procedure provided with the tester. This procedure applies a vibration of 1 mm amplitude for 90 sec to 2 grams of toner on a set of nested sieves that are 150, 75 and 45 μm in size, respectively, from top to bottom (Fig. 1). Humidity was not controlled, but was at lab ambient, which varied between about 40 to 60% RH during these tests. The percent cohesion is calculated as:

$$\text{percent cohesion} = 50 \bullet A + 30 \bullet B + 10 \bullet C \quad (1)$$

A, B and C are the toner weights left on each screen, respectively. Reproducibility was typically within 5% of the value (example, 60 ± 3% cohesion), or ±1% cohesion, whichever is larger. Equation 1 applies a weighting factor that is decreasing as the screen size decreases. Thus toner left on a smaller sieve is weighted in the calculation less than toner left on a larger screen. There will be some discussion later regarding the reasons for this weighting.

Table I lists the toners used, and Table II lists the surface metal oxide additives. The toner additives were blended onto the toners at 24 k rpm using a coffee mill.

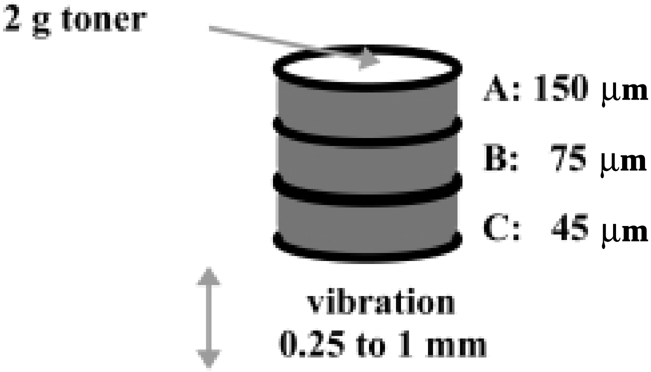

Figure 1. Powder cohesion test setup.

Original manuscript received March 12, 2001

▲ IS&T Member

* Author to whom correspondence should be addressed.

Previously presented at IS&T's NIP16: International Conference on Digital Printing Technologies, October 15-20, 2000, Vancouver, B.C. Canada.

TABLE I. Base Toner Particles

Toner ID	Resin ID	Pigment type	Pigment loading (wt %)
A1–A3	1	unoxidized carbon black	6.0
B1–B5	2	cyan	4.0
C	3	none	0
D	3	oxidized carbon black	4.2
E	3	oxidized carbon black	7.2
F	3	unoxidized carbon black	4.7
G	3	unoxidized carbon black	19.3
H	3	magenta	6.0
I	3	cyan	6.0
J1, J2	4	cyan	6.0
K1,K2	5	none	0

TABLE II. Flow Additives

Additive	Base Oxide	Treatment	Hydrophobic	H-Bonds
Degussa A380	7 nm SiO_2	none	no	yes
Degussa R812	7 nm SiO_2	HMDS	yes	no
Degussa MOX170	15 nm SiO_2	none	no	yes
Degussa R972	16 nm SiO_2	DMCS	yes	no
Degussa TT600	40 nm SiO_2	none	no	yes
Degussa P25	21 nm TiO_2	none	no	no
		HMDS	yes	no
Degussa Al2O3	20 nm Al_2O_3	none	no	no
		HMDS	yes	no
A*	100 nm	*	no	no

* Proprietary

HMDS = $((CH_3)_3SiN)_2$; DMCS = $(CH_3)_2SiCl_2$

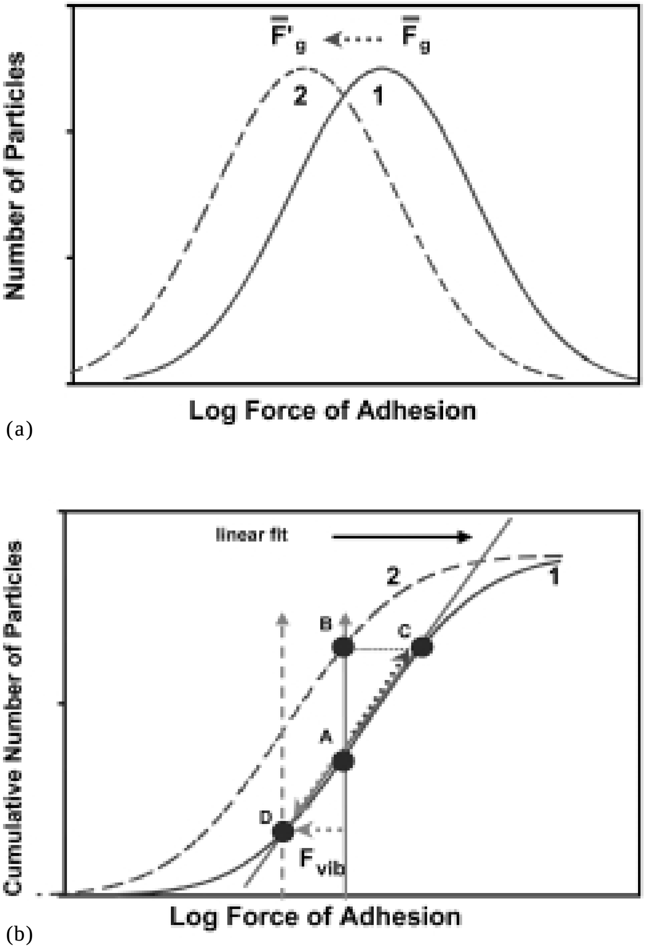

Figure 2. Relationship between log normal toner force distribution and Hosokawa powder cohesion test. Two powders of different average interparticle forces are shown: (a) Log normal force distribution; (b) cumulative log normal force distribution.

Results and Discussion

Powder Cohesion Test and Interparticle Forces

To obtain a quantitative understand of interparticle forces, it is first necessary to establish how the percent cohesion measured by the Hosokawa relates to interparticle forces, and to make this relationship as quantitative as possible. The literature is silent on this issue, despite the wide use of this technique, except for Carr's assertion[7] that there is a relationship between adhesive force and Hosokawa cohesion. The intent of the following discussion is to establish a plausible model of how this relationship might arise, and what the relationship is. It is not the intent of the current article to prove this model, but this will be the subject of a following article. First, a sample of toner consists of an ensemble of agglomerated particles. This is obvious from any micrograph of a toner without flow additives, which typically shows particles clustered together like a bunch of grapes. It is assumed that the toner ensemble cohesion follows a log normal (or Gaussian) distribution as in Eq. 2 (and Fig. 2a).

$$N_F = \frac{N_0}{\sqrt{2\pi}\ \sigma} \exp\left(\frac{(\log F - \overline{\log F})^2}{2\sigma^2} \right) \qquad (2)$$

The latter is a reasonable assumption: a log normal rather than a normal distribution is indicated as the cohesive force cannot be less than zero, which would be possible with a normal distribution. The assumption is that the particles are uncharged and thus there is no electrostatic interaction, as electrostatic interactions could be negative for charge particles of like sign. Thus, in the presence of electrostatic interactions it is not impossible that some particles could have a negative cohesive force between them. In Eq. 2, F is the magnitude of a cohesive force interaction between toner particles, and N_F is the number of particles that experience that cohesive force, out of a total number of particles, N_o. Also $\overline{\log F}$ is the mean of log F, i.e., the logarithm of the geometric mean value of F, $\overline{F}_g$.

Figure 2a shows the log normal distribution for a sample **1** with average cohesion $\overline{F}_g$ and a sample **2** having an average cohesion of $\overline{F}'_g$. Both samples have the same distribution width. For the purposes of understanding the cohesion on a single Hosokawa screen, it is more convenient to use the cumulative log normal distribution, shown in Fig. 2b, which is just the integral of Eq. 2. The screen vibration applies a defined vibrational force, F_{vib} to either of these samples, shown by the solid vertical line in Fig. 2b. All particles on the cohesion distribution curve that are below this value of F_{vib} (to the left of the vertical solid line) will pass through the screen. Any particles that are higher (to the right of the vertical solid line in Fig. 2) than this applied force will remain behind on the screen and will be weighed. The cohesion measured in the Hosokawa test will decrease as the amount left on this screen decreases. Now, suppose that the vibration is held fixed at this level, so that this constant force is applied, but now replace the more cohesive sample **1** by the less cohesive sample **2**. Clearly the amount of toner that passes the screen will increase, and the amount left will decrease (the intersection of F_{vib} on the distribution curve "moves" from A to B in Fig. 2b, so that more particles will be able to pass through the screen. So qualitatively this model makes sense. Similar, if the vibration is decreased for sample **1** (F_{vib} decreases, moving to the left in Fig. 2), the amount of toner that collects on the screen will increase, as the F_{vib} line "moves" along the distribution curve from point A to point D in Fig. 2b. In terms of the Hosokawa measured percent cohesion (the weight of toner left on a screen), the F_{vib} is thus derived to be equal to the force of cohesion between toner particles.

How can this derived relationship be converted into a quantitative relationship that describes the observed cohesion that we will measure? To do this, it is shown later in this article that there is a linear relationship between the measured Hosokawa percent cohesion, and the theoretically derived interparticle forces. It is necessary to show that the model in Eq. 2 and Fig. 2 should indeed produce a linear relationship between the measured percent cohesion and the force separating the particles, F_{vib}. This can be done with basic calculus, using the extended mean value theorem of Lagrange (often called Taylor's formula). The basic idea is that we can approximate any function (that has continuous derivatives), such the Gaussian function in Eq. 2, for any point x that is not too far from some constant chosen point, a:

$$f(x) = f(a) + f'(a) \bullet (x - a) + \text{higher order terms} \quad (3)$$

or, ignoring the higher order terms, simply:

$$f(x) = m\,x + b, \text{ where } m = f'(a) \text{ and } b = f(a) - f'(a) \bullet a \quad (4)$$

Equations 3 and 4 obviously represent a linear relationship, a reasonable approximation if x and a are not too different. How close x must be to a depends on where the point a is chosen on the curve. The simplest way to find an approximately linear relationship is to simply fit a linear expression to the integral of Eq. 2, as shown in Fig. 2b. As long as the distribution is relatively narrow, the linear fit will be a very good one over a significant part of the distribution, as it is in Fig. 2b (this particular distribution has a value σ that corresponds to about a factor of 2 in cohesive force).

To confirm that there is now a linear relationship between the cohesion (the number of particles left on the screen), and the force of adhesion, Fig. 2b can be analyzed. The vibrational force (given by the solid vertical line) is fixed at a constant value. Replacing the more cohesive sample **1**, by the less cohesive sample **2**, results in the intersection of F_{vib} on the distribution curve "moving" from A to B in Fig. 2b. Thus, the amount of toner collected on the screen, proportional to the percent cohesion on that screen, decreases linearly from point A to point C. Similarly, if the vibration is decreased for sample **1**, the amount of toner that passes through the screen will increase linearly from point A to point D, as the F_{vib} line "moves" along the distribution curve from point A to point D.

Clearly, this cohesion test will only work if the applied force is within the toner cohesive force distribution, not too far away from the mean value, and will only remain linear over some limited range. If it is too high or too low, then the Hosokawa test becomes insensitive to cohesion, as either most of the toner passes through the screen, or essentially none does. The problem then is to keep the Hosokawa test in the linear range over a wide distribution of cohesion force. Carr[7] has been clever in using different size screens. It is clear that a smaller screen requires a larger force to pass the toner (in the Hosokawa measurement, toner that easily passes through the largest screen on the top, will not pass through a smaller screen, unless the vibration force is increased). Even if all the toner passes one screen, the smaller screen below can partition toner in its linear range, extending the measurement range. Essentially when the toner flows too well through the largest screen, going out of the linear range, the amount of toner collected on that screen is very small, and no longer changes very much with the cohesion of the toner (the cumulative distribution curve becomes insensitive to the adhesive force). However, the toner will enter into the linear range of the second screen below. Again, when the second screen is out of its linear range, the third screen takes over. By proper choice of screen sizes and weighting factors the linear range of the test can be maximized which is what Carr has done empirically.

There is an assumption, that the width of the cohesive force distribution is constant. For example, narrowing the distribution results in an apparent lower cohesion for the conditions in Fig. 2, even if is unchanged. This too is compensated by different size screens, at least if there is toner on more than one screen.

Overall, there is reason to expect an approximately linear relation between Hosokawa cohesion and interparticle forces, provided that there is toner on more than one screen. This is true for the measurements to follow, except for the lowest values of cohesion, where there is toner only on the last, smallest screen.

Surface Coverage of Additives on Toner

Oxide surface coverage was estimated assuming a spherical oxide primary particle of radius r, and a spherical toner of radius, R. Equation 5 assumes the particles pack in[9] hexagonal close packing. For 100% surface coverage:

$$\text{wt\% additive} = 100 \bullet \frac{2 \bullet \pi}{\sqrt{3}} \bullet \frac{\rho_a \bullet r}{\rho_t \bullet R} \quad (5)$$

In fact, oxides are fractal, fused aggregates of primary spherical particles, which are not broken down during toner blending. Thus, while primary sizes are often quoted, the aggregate on the toner surface is larger: 300 to 500 nm. Due to the fractal architecture these particles will not cover the entire toner surface expected, as shown in Fig. 3.

Van der Waals Forces

All materials are subject to Van der Waals forces, which depend on instantaneous polarization of electrons in one material due to electromagnetic interaction with electrons in another material, as derived by Lifshitz[10]:

$$F_V = \frac{\hbar\varpi r}{16\pi L^2} \quad (6)$$

(10^{-11} to 10^{-13} ergs) depends on the materials and intervening medium ($\varepsilon_{materials}$, ε_{medium}, $n_{materials}$ and n_{medium}, where n = refractive index and ε = dielectric constant), is

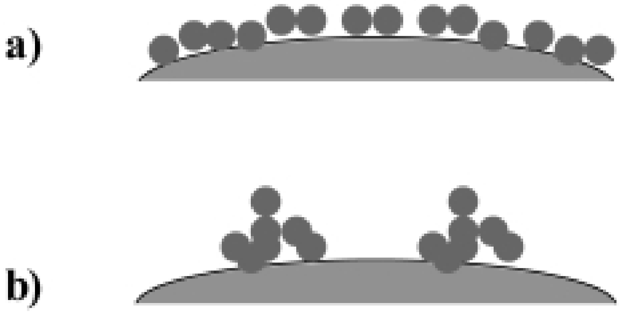

Figure 3. Additives on surface of toner after blending: (a) theoretical 100% coverage with perfect primary spheres of flow additive; (b) coverage with real fractal aggregates of spheres of flow additive at same loading.

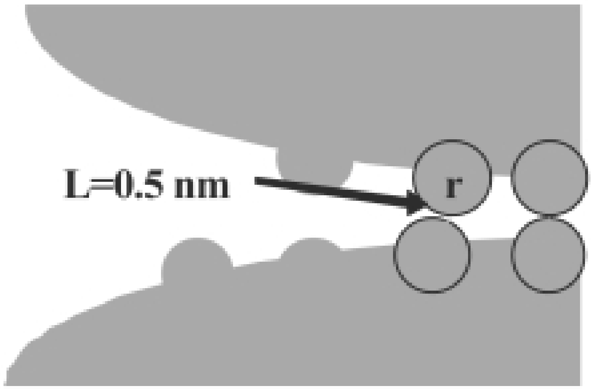

Figure 4. The contact of toner particles at asperities.

Planck's constant, L is the Van der Waals contact distance (≅0.5nm), and r is the contact radius of the curvature from surface asperities. If there are surface additives then r is the radius of the oxide *primaries*, which is the radius of curvature at the interparticle contact (not the overall size of the *aggregate*). Of the three primary forces we discuss, Van der Waals forces are the weakest, and will contribute the least to the cohesive forces when either capillary or H-bonding forces are present.

Capillary Forces

Water on surfaces creates capillary forces.[11–13] Water is in a pendular state on toner (Fig. 5), as there are less than a few monolayers (0.35 nm/monolayer[13]). The water is insufficient to bridge asperities (which are 50 to 100 nm for bare toner, or 7 to 50 nm with flow aid, as shown later). The water meniscus creates a force:[11–13]

$$F_{capillary} = 2\ \pi\ r\ \sigma_z\ (1 - L/2) \tag{7}$$

Here σ_z is the tensile strength of water (9.8×10^7 dynes/cm^2) and l = thickness of the water layer. Capillary forces will be larger than Van der Waals forces.

Hydrogen Bonding

Toner surface groups that form hydrogen bonds will create an interparticle force. Figure 6 shows the contact of two silica primaries of radius, r. Interparticle H-bonds form between –OH groups within an area, $S_{H\text{-}bond}$, of "radius", a, from the "contact". Outside this area the water layer separation, $2L$, is too large for an H-bond, due to surface curvature. Because $a << r$, $S_{H\text{-}bond} = \pi a^2$, $s = r\theta \cong h \cong a$, $\sin\theta \cong \theta$, and $L = h \bullet \sin(\theta/2)$.

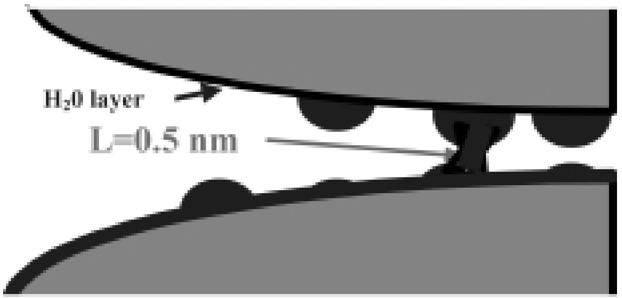

Figure 5. Pendular water between toner asperities.

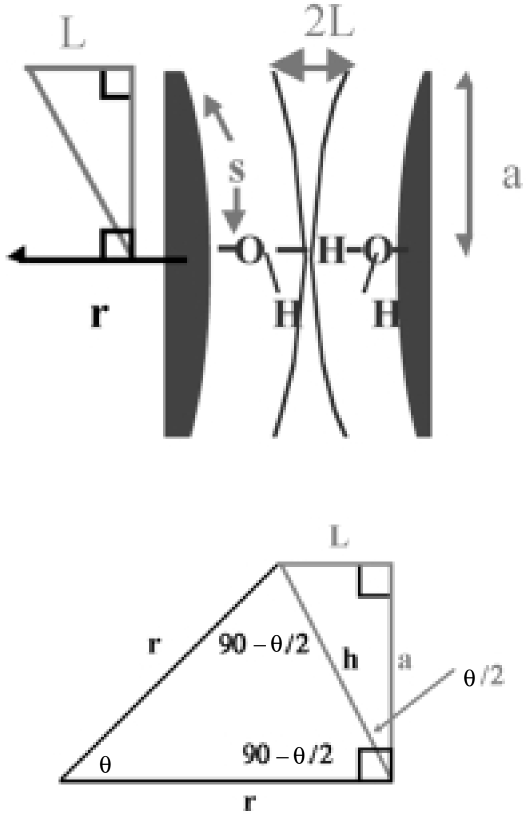

Figure 6. Geometry for interparticle H-bond area in Eq. 6.

$$S_{H\text{-}bond} = \pi\ a^2 = \pi\ (r\theta)\ (L/\sin(\theta/2) = 2\pi\ r\ L \tag{8}$$

The adhesive force is ($\Gamma_{H\text{-}bond}$ = surface area density of H-bonds, and $f_{H\text{-}bond}$ = bond strength):

$$F_{H\text{-}Bond} = 2\ \pi\ L\ \Gamma_{H\text{-}Bond}\ f_{H\text{-}Bond}\ r \tag{9}$$

If the surface chemistry allows high H-bond densities, where there are H-bonds to each –OH group on an untreated silica, for example, it is anticipated the H-bond forces will be similar in magnitude to capillary forces, both of which are stronger than Van der Waals forces.

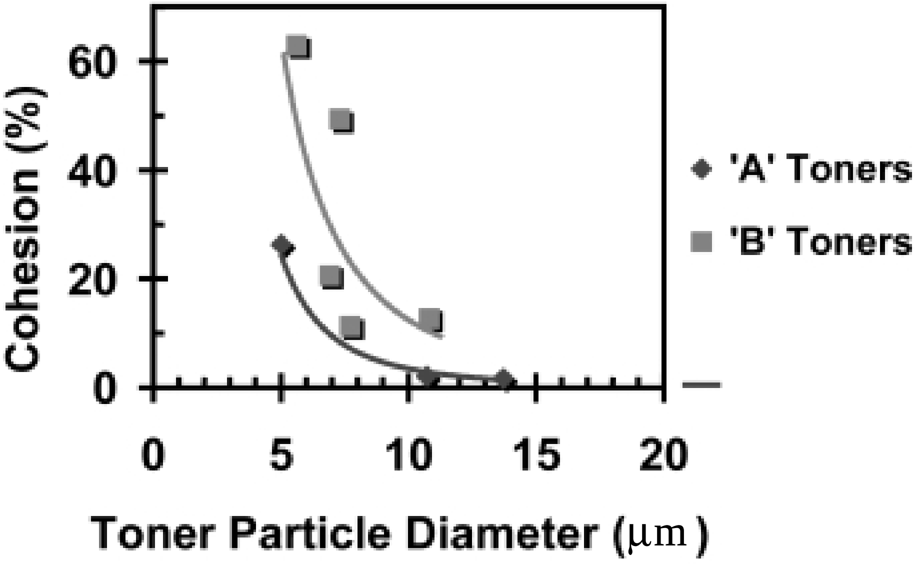

Figure 7. Powder cohesion with toner particle size.

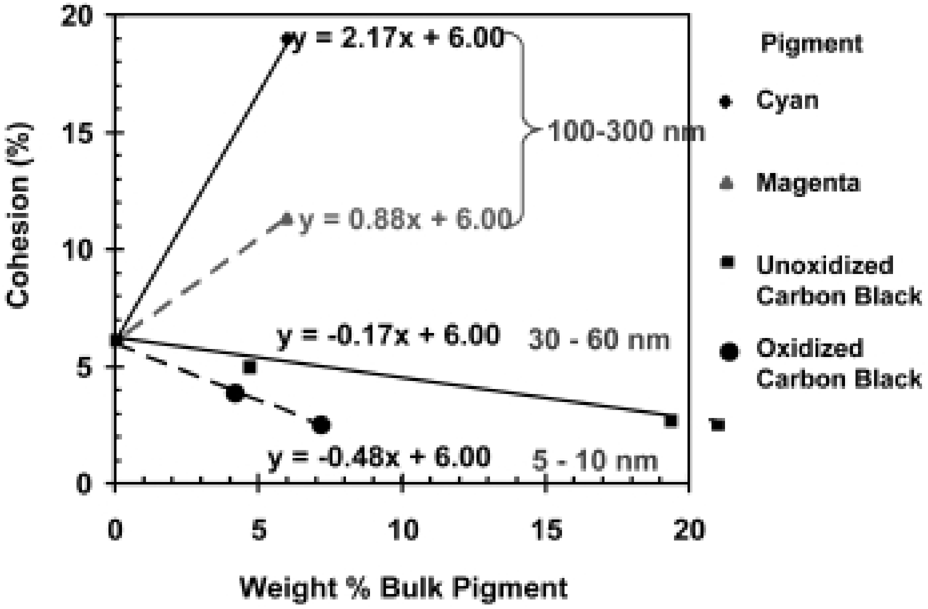

Figure 8. Toner cohesion with pigment type and loading.

Overall, all interparticle forces, whatever the origin, are linear in the asperity radius: larger asperities result in larger forces.

Toner Powder Flow Cohesion Tests

Why do we now worry at all about toner flow when early toners had no flow additives, yet functioned well? There are two clear reasons for this change in attitude to flow. Fig. 7 shows one reason, illustrated by two toner series. In each series decreased particle size shows a dramatic cohesion increase. Thus the current trend to small toner increases the need for flow additives.

Figure 8 shows how cohesion changes with pigment loading. If cohesion is controlled by the asperity size, as shown in the derivation of the adhesion forces (as discussed above), then a bare "parent" toner particle will have a certain "natural" asperity size, representing its surface roughness. If the pigment particle is expressed on the toner surface, then the pigment creates new surface asperities on the toner. If the pigment size is larger than the initial toner asperity size, then flow will be worse than without pigment, as defined by Eqs. 6, 7 and 9. The cohesion will be linear with loading of pigment (assuming the pigment expressed on the toner surface is proportional to the amount in the bulk). If the pigment size is smaller than the initial asperity size then the cohesion will be reduced with more pigment. For small carbon blacks, less than 60 nm in primary size (black toners), cohesion drops linearly with pigment loading. Color pigments are larger than these carbon blacks, and show a linear **increase** in cohesion with loading. Thus, the cohesion as a function of pigment size and loading is consistent with Eqs. 6, 7 and 9, assuming the bare toner asperity size is between 60 to 100 nm

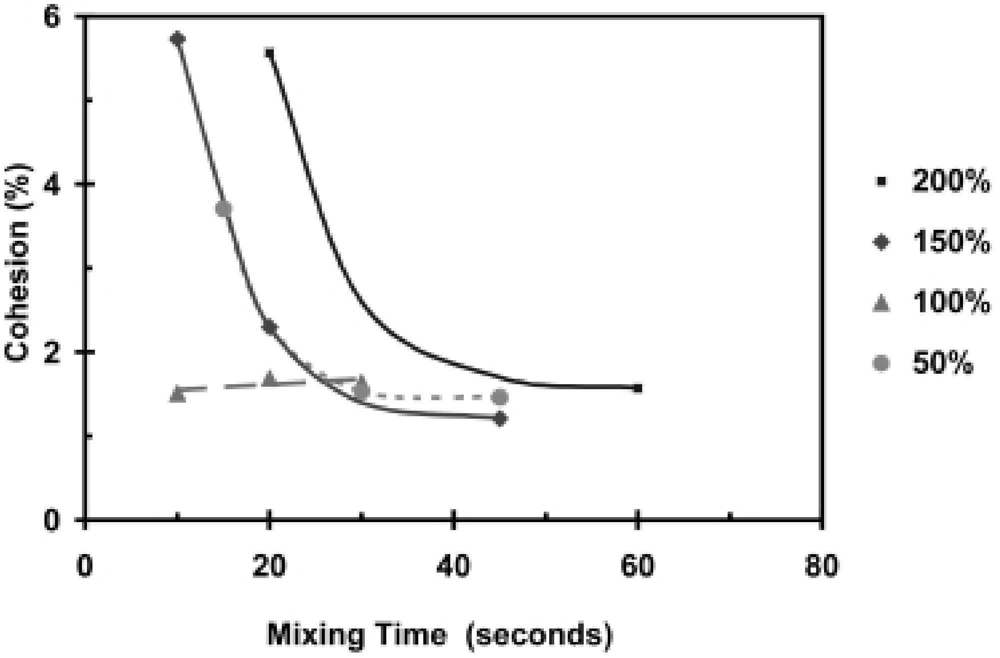

Figure 9. Coffee mill blending of R812 on toner J2.

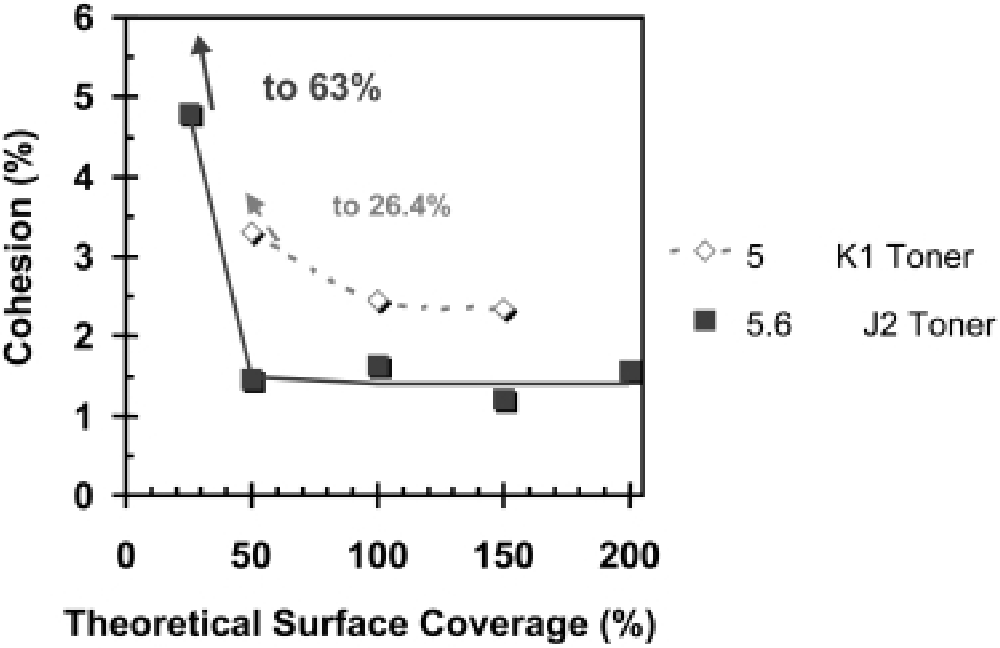

Figure 10. Optimal cohesion with additive coverage.

for these toners: smaller pigments are flow aids, larger pigment particles are "cohesives".

Figure 9 shows toner cohesion with additive blending time for various theoretical coverages (Eq. 5), based on the primary size of the flow additive. At any coverage, from 50% to 200%, the cohesion ultimately reaches the same cohesion at long blend times. At 50% coverage the cohesion drops rapidly. At 100% coverage, cohesion remains low over all blend times studied, even at the short blend times, while above 100% coverage, cohesion again drops rapidly. This behavior is reasonable. If there is barely enough additive to cover the toner surface, then good surface coverage requires perfect dispersion; if there is sufficient additive a poor dispersion is tolerable, as even a poor dispersion can still cover the surface. Above the required loading for good coverage, excess additive will be loose, not on the toner surface, as confirmed by SEM. This impedes flow until the loose additive is blended onto the surface (R812 silica alone, without toner, has a cohesion of 60%!).

Figure 10 shows the cohesion, measured at the optimal blend time for each surface coverage (from Fig. 9). This optimal cohesion is independent of coverage, from 50% to 250%. Only at 25% coverage is cohesion higher. Thus, while it takes longer to blend at 50% or 250% theoretical coverage, equivalent flow to 100% coverage is ul-

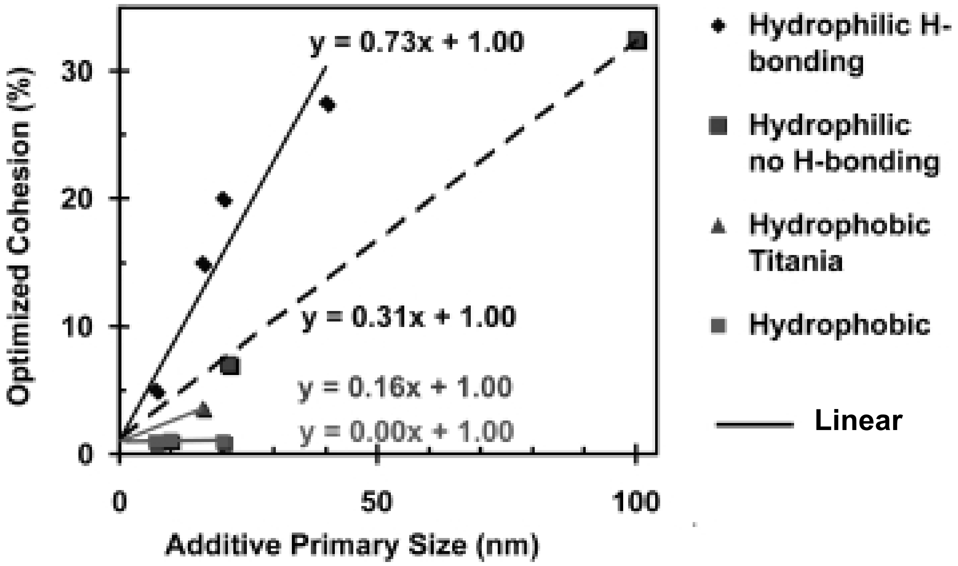

Figure 11. Cohesion with additive size and type on toner J2.

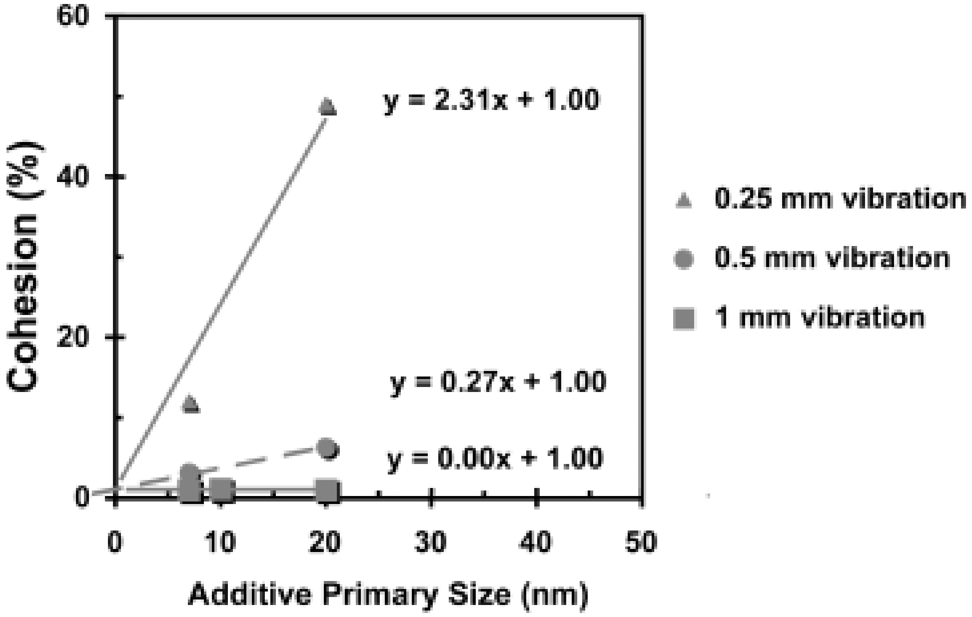

Figure 12. Cohesion with hydrophobic additives.

timately obtained. A second toner (blend optimization not shown) does show reduced cohesion between 50% and 100% coverage. While it is not clear why the toners behave differently, in both cases near 100% coverage, based on Eq. 5, they do indeed give optimal flow. Seeing optimal cohesion near 100% coverage does not necessarily mean that the toners are dispersing like primary particles. It may simply be that even at less than 100% coverage there is sufficient additive to reduce cohesion to the optimal value. Even if two toner particles only have partial 50% coverage it is clear that very few contacts between the particles would not involve additive to additive contacts.

Figure 11 shows the optimal cohesion (blending data not shown) at 100% oxide coverage, grouped according to oxide surface properties. Hydrophilic additives capable of H-bonding (untreated oxides with surface OH groups that form strong H-bonds) have the largest interparticle forces, because the adhesion force is produced from all three primary forces: H-bonding, Van der Waals and capillary. Cohesion increases linearly with the additive primary radius, as expected from Eqs. 6, 7 and 9. Lower cohesion arises with hydrophilic additives that do not form strong H-bonds (such as untreated titania, for example). These additives also show the expected linear increase in cohesion with additive primary size (Eqs. 6 and 7), but with reduced size dependence (by a factor of 2.5) due to the lack of H-bonds. The lowest cohesion is obtained with hydrophobic oxides. These are silicas treated to render them hydrophobic, removing any OH groups that might form H-bonds.[1] The cohesion with these additives is so good that the lower test limit is exceeded. To extend the test a lower vibration amplitude is needed.

Figure 12 shows the effect of reduced vibration on hydrophobic additives. As the vibration decreases from the standard 1 mm vibration, cohesion increases rapidly. Figure 12 shows that cohesion does increase linearly with additive size as expected for Van der Waals' forces (Eq. 3).

Thus, all three types of surface chemistries, categorized by the type of forces that are involved, show the anticipated increase in cohesive force, and thus decrease in toner flow, with increasing additive primary size (radius of curvature at the contact point), as expected from the theory for these forces. Further, as anticipated, those additives with both H-bonding and capillary forces will have the highest cohesion, while those with only Van der Waals forces will have the lowest cohesion.

Conclusions

A full quantitative model of a toner cohesion force distribution has been proposed and verified, based on a log normal cohesive force distribution and has the theoretical derivation of the three primary interparticle cohesive forces: Van der Waals, capillary, and hydrogen bonding forces. Toner flow with surface additives depends on the presence of these forces, and for all three, the force is determined by the nano-geometry of contact, defined by the toner asperity size. Toner surface additives act as small asperities. Asperity size is important as it defines the radius of curvature at the contact point between two toner particles. The radius of curvature of the contact for metal oxide additives is thus determined by the primary size of the toner additive, not the size of the fractal aggregate. It is shown that the toner cohesion increases linearly with the primary additive size, no matter what combination of H-bonding, capillary and Van der Waals forces are expressed on the additive surface. This is shown to be true only if there is enough flow additive to give sufficient surface coverage for optimal flow, and if there is sufficient blending to disperse the additive on the toner surface. Overall cohesion decreases with increasing hydrophobicity, decreasing hydrogen bonding, and decreasing size.

References

1. A. Stubbe, *Proceedings of IS&T 7th International Congress on Advances in Non-Impact Printing Technologies*, IS&T, Springfield, VA, 1991, p. 240.
2. A. R. Gutierrez, H. T. Nguyen and A. F. Diaz, *Proceedings of IS&T 8th International Congress on Advances in Non-Impact Printing Technologies*, IS&T, Springfield, VA, 1992, p. 122.
3. R. P. N. Veregin, C. P. Tripp and M. N. V. McDougall, *Proceedings of IS&T 10th International Congress on Advances in Non-Impact Printing Technologies*, IS&T, Springfield, VA, 1994, p. 131.
4. C. P. Tripp, R. P. N. Veregin, M. N. V. McDougall, and D. Osmond, *Langmuir* **11**, 1858 (1995).
5. R. P. N. Veregin, C. P. Tripp, M. N. V. McDougall, and D. Osmond, *J. Imaging Sci. Technol.* **39**, 429 (1995).
6. H. Akagi, *Proc. SPIE* **138,** 1670 (1992).
7. R. L. Carr, *Chemical Eng.* Jan. 18 and Feb. 21 (1965).
8. C. P. Tripp, R. P. N. Veregin, and D. Osmond, unpublished data.
9. N. Pilpel, *Manufacturing Chemist and Aerosol News* **41**, 19 (1970).
10. J. N. Israelachvili, *Intermolecular and Surface Forces*, Academic Press, London, 1985.
11. M. Chikazawa, T. Yamaguchi and T. Kanazawa, *Proc. Int. Symp. Powder Technol.* Kyoto, Japan, 1981 p. 202.
12. T. Kohler and H. Schubert, *Part. Part. Syst. Charact.* **8**, 101 (1991).
13. M.C. Coelho and N. Harnby, *Powder Technol.* **20**, 201 (1978).